PHYSICAL REVIEW A **71**, 033203 (2005)

Energies and density distributions of $(^4He)_N$ clusters doped with $Br_2(X)$: A Hartree-like approach

M. P. de Lara-Castells,* D. López-Durán, G. Delgado-Barrio, and P. Villarreal
Instituto de Matemáticas y Física Fundamental (CSIC), Serrano 123, E-28006-Madrid, Spain

C. Di Paola and F. A. Gianturco
Department of Chemistry and INFM, University of Rome La Sapienza, Piazzale A. Moro 5, 00185 Rome, Italy

J. Jellinek
Chemistry Division, Argonne National Laboratory, Argonne, Illinois 60439, USA
(Received 22 October 2004; published 8 March 2005)

Energies and density distributions of the helium atoms in $Br_2(X)$-$(^4He)_N$ clusters are calculated using a quantum "Hartree-like" approach in which the dopant molecule and the ^4He atoms play the role of the nuclei and electrons, respectively, of the original Hartree formulation. A detailed generalization of the methodology is presented. The validity of this treatment is assessed by comparing energies and density distributions for $N=2$ up to $N=18$ with those obtained by performing quantum diffusion Monte Carlo (DMC) calculations. The present Hartree model shows good agreement with the DMC calculations, the main difference being that the DMC density distributions of the He atoms are more isotropic than those generated via the model. The treatment is extended to larger (up to $N=60$) clusters and saturation effects are analyzed and discussed.

DOI: 10.1103/PhysRevA.71.033203 PACS number(s): 36.40.Mr, 31.15.Ar, 33.20.Fb, 33.80.Gj

I. INTRODUCTION

Recent advances in experimental investigations of spectroscopic properties of molecules in helium droplets have raised new and challenging questions on the role of the "quantum environment" [1]. The experiments produced a number of interesting observations; for example, measurements of Grebenev *et al.* [2] on the carbonyl sulfide (OCS) molecule solvated by helium atoms revealed different spectra of the dopant molecule depending on the fermionic or bosonic character of the solvent. The spectroscopic probe of the impurity species indicates free-rotor-like behavior in ^4He droplets—although with an increased moment of inertia—whereas in ^3He droplets the spectrum of the dopant has an unstructured broad profile. Adding a small number of ^4He atoms (~ 60) to the fermionic solvent leads to recovering the structured spectrum of the solvated molecule, a feature which was interpreted as a manifestation of superfluidity on the microscopic scale [2]. A number of additional experiments on small- and intermediate-sized doped helium clusters [3–6] based on helium nanodroplet isolation (HENDI) spectroscopy [7] have been performed recently.

Theoretical and computational studies of the cluster solvation phenomenon pose a number of challenges. The systems may be too small for a statistical treatment and too large for a detailed (nuclei+electrons) structural and dynamical analysis. A practical approach for describing doped bosonic helium clusters is to use variational, diffusion, and path integral Monte Carlo (MC) methods (see, e.g., Refs. [8,9]). The latter represents the most accurate computational approach. The most obvious difficulty in extension to fermionic clusters is the nodal structure of the wave function which causes the local energy to become infinite during the MC walk. A quantum-chemistry-type methodology in which the dopant molecule and the ^3He atoms play the role of the nuclei and electrons, respectively, was first proposed and implemented only for the cases of one and two ^3He atoms by Jungwirth and Krylov [10]. Heidenreich and Jortner [11] extended the approach to bosons and carried out configuration interaction calculations for anthracene·He_N ($N=1,2$) complexes [11]. As compared to alternative approaches based on density functional theory (see, e.g., Ref. [12]) an appealing advantage of such a quantum-chemistry-type treatment is that it also provides the wave functions which allow one to simulate the spectra and other possible observables of the dopant molecule in helium clusters.

We have recently used this approach and performed many-body Hartree or Hartree-Fock calculations in order to simulate the vibrotational Raman spectra of bosonic, fermionic, and mixed ($N=2$ up to $N=18$) $Br_2(X)$-He_N clusters [13,14]. In ^4He clusters the spectrum of Br_2 resembles that of the isolated molecule with well-defined rotational branches. In ^3He clusters the high-energy degeneracy of different spin-multiplicity states leads to an overlap of several lines, resulting in an unstructured broadband. As ^4He atoms are added to the cluster, the degeneracy is gradually reduced and the profile of the spectrum evolves into that of the bosonic case.

The objective of this paper is to present details and a generalization of the methodology used as well as to extend the study to clusters of larger sizes. In addition, we provide an assessment of the performance of the Hartree model by comparing both its energetics and structure results with those arising from "exact" diffusion MC (DMC) calculations [15].

The paper is structured as follows: Sec. II discusses the methodology and technical details. Results of the energetics and helium density distributions in $Br_2(X)$-$(^4He)_N$ (N

*Author to whom correspondence should be addressed. Electronic address: delara@imaff.cfmac.csic.es

$=1,18$) clusters are presented in Sec. III, where we also compare the model with the DMC calculations. In this section we also present results obtained applying the Hartree model to larger clusters and analyze saturation effects. In Sec. IV, we provide a summary and discuss future directions.

II. COMPUTATIONAL METHOD

A. Hamiltonian: Born-Oppenheimer approximation

We first define the nuclear Hamiltonian for the system as consisting of the Br_2 molecule solvated by N helium atoms. Using satellite coordinates $(\mathbf{r},\mathbf{R}_k)$, where $\mathbf{r}$ is the vector joining the two bromine atoms and $\mathbf{R}_k$ are vectors from the diatomic center of mass to the different helium atoms, this Hamiltonian can be written as

$$H^{(N)} = -\frac{\hbar^2}{2m}\frac{\partial^2}{\partial r^2} + U(r) + \frac{\mathbf{j}^2}{2mr^2} + \sum_{k=1}^{N} h_k(\mathbf{R}_k,r) + \sum_{k<l} V_{kl}(|\mathbf{R}_k-\mathbf{R}_l|) - \frac{\hbar^2}{m_{Br_2}}\sum_{k<l}\boldsymbol{\nabla}_k\cdot\boldsymbol{\nabla}_l, \tag{1}$$

where the first three terms correspond to the Hamiltonian of the free diatomic molecule with m, $\mathbf{j}$, and U being the diatomic reduced mass, the angular momentum associated with $\mathbf{r}$, and the Br_2 intramolecular potential, respectively. The fourth term consists of N triatomic He-Br_2 Hamiltonians which can be written as

$$h_k(\mathbf{R}_k,r) = -\frac{\hbar^2}{2\mu}\frac{\partial^2}{\partial R_k^2} + \frac{\mathbf{l}_k^2}{2\mu_\epsilon R_k^2} + W(r,R_k,\theta_k), \tag{2}$$

where μ is the reduced He-Br_2 mass, $\mathbf{l}_k$ is the angular momentum associated with $\mathbf{R}_k$, and W is the weak atom-diatom intermolecular interaction potential, which depends on the (r,R_k) distances and the angle between the $\mathbf{r}$ and $\mathbf{R}_k$ vectors. In the fifth term of Eq. (1), V_{kl}, represents the pair interaction potential between the kth and lth helium atoms. Finally, in the sixth term, $(-\hbar^2/m_{Br_2})\nabla_k\cdot\nabla_l$, is the kinetic energy coupling between the kth and lth helium atoms.

Choosing a body-fixed (BF) coordinate system with the Z axis parallel to $\mathbf{r}$ and a fixed value of the intramolecular distance r, the ground state of the bound cluster of N helium atoms is obtained by solving the Schrödinger equation

$$\left[\sum_{k=1}^{N} h_k + \sum_{k<l} V_{kl} - E_\Lambda^{(N)}(r)\right]\Phi_\Lambda^{(N)}(\{\mathbf{R}_k\};r) = 0, \tag{3}$$

in which the r-dependent eigenvalues are labeled by Λ, the projection of the orbital angular momentum $\mathbf{L}=\sum_{k=1}^{N_\epsilon}\mathbf{l}_k$ on the molecular axis. This representation is equivalent to the Born-Oppenheimer approximation in which the Br_2 molecule and He atoms play the role of the nuclei and electrons, respectively. For a total angular momentum $\mathbf{J}=\mathbf{j}+\mathbf{L}$ with a projection onto the BF Z-axis Λ and neglecting the Coriolis couplings, the effective Hamiltonian of the dopant can be written as

$$H_N^{eff} = -\frac{\hbar^2}{2m}\frac{\partial^2}{\partial r^2} + U(r) + E_\Lambda^{(N)}(r) + \frac{\hbar^2}{2mr^2}G, \tag{4}$$

where $G=\langle\mathbf{j}^2\rangle$ is given by [16]

$$G = J(J+1) + L(L+1) - 2\Lambda^2. \tag{5}$$

Since the orbital angular momentum L is not a good quantum number, we average it over the helium total angular momentum distributions:

$$\langle L^2\rangle \approx \sum_{L_N} P(L_N)L_N(L_N+1), \tag{6}$$

where the probabilities, or weights, $P(L_N)$ are calculated from the N-boson ground-state wave function at the Br_2 equilibrium distance r_e (see Appendix B):

$$P(L_N) = \langle L_N|\Phi^{(N)}(r_e)\rangle^2. \tag{7}$$

We can then solve the Schrödinger equation for the "distorted" dopant molecule with the N helium atoms bound to it:

$$\left[H_N^{eff} - \epsilon_{J\Lambda v}\right]\chi_{J\Lambda v}(r) = 0, \tag{8}$$

where v is the vibrational stretching quantum number. Within this approximation, the total wave function can be written as

$$\Psi \approx \mathcal{D}^{J^*}_{M\Omega}(\varphi_r,\theta_r,0)\Phi_\Lambda^{(N)}(\{\mathbf{R}_k\};r)\chi_{J\Lambda v}(r), \tag{9}$$

where $\mathcal{D}^J_{M\Omega}$ is the Wigner rotation matrix that depends on the angular polar components (θ_r,φ_r) of $\mathbf{r}$ in a space-fixed (SF) frame.

B. Hartree-like approach

In order to solve Eq. (3) we have used a Hartree-like approach. This means that the wave function of the N bound helium atoms is taken to be a symmetrized Hartree product ("permanent") of single-particle wave functions. If N_i spinless bosons occupy the same one-particle orbital of index i, the total wave function of the system of $N=\sum_i^M N_i$ $(M\leqslant N)$ bosons can be expressed as

$$\Phi^{(N)}_{(N_1,\ldots,N_M)} = \frac{1}{\sqrt{\mathcal{N}}}\hat{\mathcal{S}}\left(\prod_{i=1}^{N_1}\psi_1(\mathbf{R}_i;r)\prod_{j=N_1+1}^{N_1+N_2}\psi_2(\mathbf{R}_j;r)\cdots \times \prod_{k=(N_1+\cdots+N_{M-1})+1}^{N}\psi_M(\mathbf{R}_k;r)\right), \tag{10}$$

where $\hat{\mathcal{S}}$ is the symmetrization operator, $1/\sqrt{\mathcal{N}}$ is the normalization factor, and $\mathcal{N}$ is the number of different Hartree products obtained by interchanging the bosons occupying different orbitals:

$$\mathcal{N} = \binom{N}{N_1}\binom{N-N_1}{N_2}\cdots\binom{N-(N_1+\cdots+N_{M-1})}{N_M}. \tag{11}$$

The energy of the N-boson system can be written as

$$E_{\Lambda}^{(N)} = \sum_{i=1}^{M} N_i \epsilon_i + \sum_{i,j=1}^{M} \frac{N_i(N_j - \delta_{ij})}{2(1+\delta_{ij})}(J_{ij} + K_{ij}), \tag{12}$$

where

$$\epsilon_i = \int d\mathbf{R}\, \psi_i^*(\mathbf{R};r) h(\mathbf{R},r) \psi_i(\mathbf{R};r) \tag{13}$$

is the average kinetic and potential energy (that of each He atom with the dopant) of a boson described by the orbital $\psi_i(\mathbf{R};r)$. The term

$$J_{ij} = \int\int d\mathbf{R}_1 d\mathbf{R}_2 |\psi_i(\mathbf{R}_1;r)|^2 V'_{12} |\psi_j(\mathbf{R}_2;r)|^2, \tag{14}$$

where

$$V'_{12} = V_{12}(|\mathbf{R}_1 - \mathbf{R}_2|) - \frac{\hbar^2}{m_{Br_2}} \nabla_1 \cdot \nabla_2, \tag{15}$$

represents the interaction between the bosonic clouds $|\psi_i(\mathbf{R}_1;r)|^2$ and $|\psi_j(\mathbf{R}_2;r)|^2$. It is equivalent to the *Coulomb integral* in electronic structure theory. Note that Eq. (15) explicitly incorporates the kinetic coupling. The term

$$K_{ij} = \int\int d\mathbf{R}_1 d\mathbf{R}_2 \psi_i^*(\mathbf{R}_1;r) \psi_j(\mathbf{R}_1;r) V'_{12} \psi_j^*(\mathbf{R}_2;r) \psi_i(\mathbf{R}_2;r) \tag{16}$$

is an analog of the exchange integral. If one considers the particular case in which each boson occupies a different orbital, Eq. (12) reduces to

$$E_{\Lambda}^{(N)} = \sum_{i=1}^{N} \epsilon_i + \sum_{i<j}^{N} (J_{ij} + K_{ij}), \tag{17}$$

which, with the exception of the sign in front of the second term on the right-hand side, is the expression for the Hartree-Fock energy of N fermions occupying N different spin-orbitals. In the other limiting case, when all the bosons are populating the same orbital, the expression for the energy simplifies to

$$E_{\Lambda}^{(N)} = N\epsilon_1 + \frac{N(N-1)}{2} J_{11}. \tag{18}$$

The orbitals are computed through a direct minimization procedure [17,18] to ensure convergence to the global minimum.

C. Basis set functions

We used a finite basis set composed of products of radial and angular functions

$$\chi^{(n\ell m)}(\mathbf{R};r) = g_n(R;r) Y_{\ell m}(\theta,\phi), \tag{19}$$

where $Y_{\ell m}(\theta,\phi)$ are spherical harmonics. The radial $g_n(R;r)$ functions are obtained by solving the Schrödinger equation corresponding to the triatomic He-Br_2 subsystem at different fixed orientations θ_n:

TABLE I. Values of the parameters used to describe the different atom-atom interaction potentials.

Interaction	D (cm^{-1})	α ($Å^{-1}$)	ρ_{eq} (Å)	γ ($a.u.^{-1}$)	V_c (cm^{-1})
$Br_2(X)$	24557.674	1.588	2.281		
He-Br(X)	19.62	1.55	3.81		
He-He	7.61	2.126	2.963	2000	11.53

$$\left[-\frac{\hbar^2}{2\mu} \frac{\partial^2}{\partial R^2} + W(R,\theta_n;r) - E_n(r) \right] g_n(R,\theta_n;r) = 0. \tag{20}$$

The set of θ_n values represents an equidistant grid of n_{max} points in the range $[0, \pi/2]$. The $g_n(R,\theta;r)$ functions were then orthogonalized using the Schmidt orthogonalization procedure.

The one-particle and two-particle integrals were evaluated analytically in the angular variables and numerically in the radial ones. The details are given in Appendix A.

D. Interaction potentials

The $Br_2(X)$ intermolecular interaction U was described by a Morse function [19]

$$U(r) = D\{1 - \exp[-\alpha(r - r_{eq})]\}^2. \tag{21}$$

The He-$Br_2(X)$ intramolecular potential W was approximated through the addition of Morse-type He-Br pair interactions [20]

$$W(r,R,\theta) = M(R_1) + M(R_2), \tag{22}$$

where R_i, $i=1,2$ are the two He-Br distances and

$$M(R_i) = D'\{1 - \exp[-\alpha(R_i - R_{eq})]\}^2 - D'. \tag{23}$$

This He-Br_2 interaction potential turned out to be highly anisotropic with its minimum in the T-shaped configuration at about -38 cm^{-1}. The binding energy of the linear orientation is about -20 cm^{-1}. In another study [15], we compared the DMC results on the energetics and the helium density distributions obtained using both the pair potentials, Eqs. (21)–(23), and a further *ab initio* evaluation of the He-Br_2 interaction [21]. In that study we have shown that as the cluster size increases, the differences in the description of the interaction with the dopant molecule become insignificant because of the increasing role of the He-He interactions. In this study we employ the simpler pairwise-additive model description.

The He-He interaction is also described by a Morse potential [22]. To avoid the divergence problem due to the strong interatomic repulsion as $R_{12} \to 0$, we truncated the potential in two different ways [12,23]: (1) by replacing V with $V' = V \exp[-\gamma V]$ ("truncated barrier" scheme) and (2) by introducing a cutoff value V_c. Both parameters γ and V_c allow for selection of the maximum repulsion at short distances. They were determined by fitting the ground-state energy to its "exact" DMC value at $N=2$. Table I displays the values of γ, V_c, and the other parameters of the different atom-atom interactions.

III. COMPUTATIONAL DETAILS, RESULTS, AND DISCUSSION

The calculations were performed with the masses (in amu) $m_{\mathrm{Br}}=78.918\,30$ and $m_{^4\mathrm{He}}=4.002\,60$. A grid of 5000 points in the range [1.5–18.5] Å was employed to solve numerically Eq. (20) using a Numerov procedure. The comparison with the DMC data was performed at the equilibrium Br-Br distance $r_e=2.281$ Å. Convergence of the energy within 0.01 cm^{-1} for cluster sizes up to $N=60$ bosons was achieved by using $l_{max}=24$, $|m_{max}|=1$, and $n_{max}=8$. For $N=2$, the initial guess for the orbitals was derived from the diagonalization of the Hamiltonian corresponding to the independent-particle approximation. From $N=4$, the results of calculations with $N-2$ bosons were used as the initial guess for the orbitals. The convergence thresholds for the eigenvalues and the total energies were set to 10^{-6} and 10^{-7} cm^{-1}, respectively.

The lowest energy was invariably found for $\Lambda=0$ and for a symmetric wave function, or sort of "Σ_g," state of the system. Table II shows the energies of the Br_2-He_N clusters computed at the equilibrium Br_2 bond length and for N bosons initially distributed over $M=1$, 2, and 3 orbitals. In contrast to the case of the fermions (Hund's rule), the lowest energies for all cluster sizes are obtained when all the bosons occupy the same orbital which corresponds to a minimum value for the projection of the bosonic angular momentum onto the molecular axis. The lowest energies are 3%–14% below those obtained with $M=2$ and 3. The relative energy differences between the various M cases are very similar for both the "barrier" and "cutoff" He-He potentials. Comparison of the results obtained with $M=1$ with the two types of truncation of the potential shows a maximal difference of 4.2% at $N=8$ and indicates that the "truncated barrier" scheme leads to larger binding energies. Inclusion of the kinetic coupling in Eq. (15) did not show a substantial effect. For example, the changes in the total energy for $M=3$ are 0.05 cm^{-1} and 0.35 cm^{-1} for $N=6$ and $N=20$, respectively. However, in the case of lighter dopant molecules the effect of the kinetic coupling might be important.

A. Test cases: Comparison with DMC calculations

In Fig. 1 we show the Hartree and DMC total energies, together with the errors for the DMC energies (within 2%), as a function of the cluster size. Details of the DMC calculations are given in Ref. [15]. It is clear from the figure that for both modified He-He potentials the agreement with the DMC results is fairly good. The maximum relative errors for the Hartree energies are found at $N=8$. They are about 11% and 14% for the "barrier" and "cutoff" truncation schemes, respectively.

In Figs. 2 and 3 the radial (left panels) and angular (right panels) helium probability density distributions around the solvated Br_2 dopant molecule obtained using DMC and Hartree computations are shown for different cluster sizes. Since the degree of anisotropy of these distributions depends on the competing effects of the dopant-He and He-He interactions and since the former is the same in both the Hartree and DMC calculations, the similarity of the distributions is a good indication of the adequacy of the He-He truncation models.

Analysis of Figs. 2 and 3 shows that for the smaller clusters the angular density distributions are highly anisotropic peaking at $\theta=\pi/2$. This is a consequence of the strong anisotropy in the helium-Br_2 potential which favors the T-shaped arrangement. The He atoms populate primarily the well associated with this arrangement up to about $N=6$. For larger N, the increasing He-He repulsion causes the density distribution to flow from a T configuration well into the other potential regions. Indications for formation of two side peaks at $\theta=\pi/4$ and $3\pi/4$ are evident for $N=12$, and these peaks are clearly present in the graphs corresponding to $N=16$ and 18. We return to this point in the discussion below.

Comparison of the "truncated barrier" angular distributions shows a difference that starts at $N=8$: the DMC distributions are less anisotropic. This difference becomes more pronounced as the cluster size increases. The Hartree calculations with the "cutoff" potential are overall in better accord with the DMC results. For $N=8$ and 10 the two distributions essentially coincide. For larger cluster sizes the DMC distributions are slightly more isotropic.

TABLE II. Energies (in cm^{-1}) of the Br_2-He_N clusters computed using the Hartree-like scheme with (a) "truncated barrier" and (b) "cutoff" He-He potentials discussed in the text. The three columns for each case represent different distributions of the bosons over the orbitals. The values correspond to the lowest-energy "Σ_g" state.

	(a)			(b)		
N	$(M=1)$	$(M=2)$	$(M=3)$	$(M=1)$	$(M=2)$	$(M=3)$
2	−35.48	…	…	−35.15	…	…
4	−67.19	−65.01	…	−65.43	−62.79	…
6	−95.35	−90.81	−86.68	−91.85	−86.44	−83.64
8	−120.50	−113.14	−107.15	−115.70	−107.30	−103.39
10	−143.49	−133.19	−131.15	−137.91	−126.24	−122.11
12	−165.00	−151.58	−151.08	−158.93	−143.58	−143.55
14	−185.30	−168.54	−167.77	−178.91	−159.42	−160.46
16	−204.54	−184.25	−186.50	−197.92	−173.85	−175.30
18	−222.82	−198.92	−201.62	−215.98	−186.91	−188.33
20	−240.29	−212.12	−218.01	−233.12	−198.65	−201.88

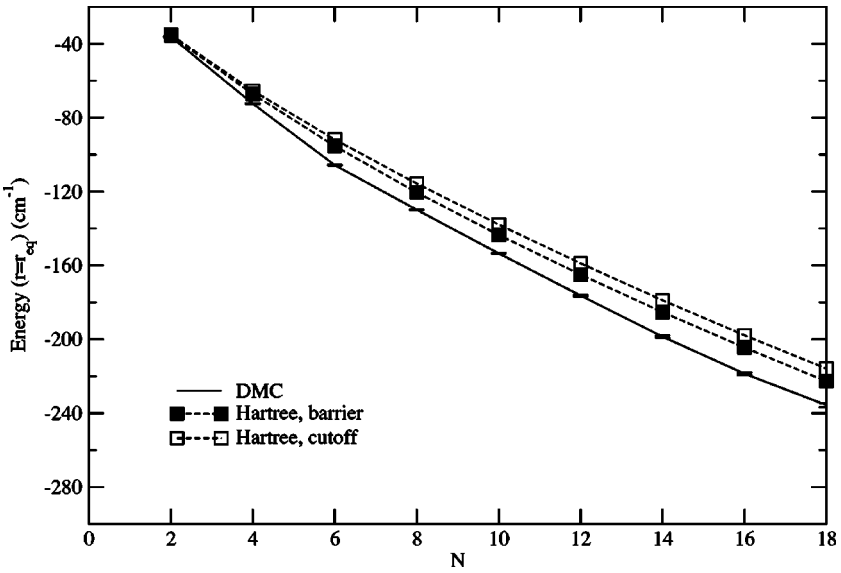

FIG. 1. Energy values (in cm^{-1}) computed within the DMC and Hartree approaches using the "truncated barrier" and "cutoff" He-He potentials discussed in the text.

Inspection of the helium radial probability density distributions around the dopant's center of mass indicates that they become more diffuse and shift to larger distances R as the cluster size increases. Thus, the DMC distribution peaks at $R \sim 4$ Å for $N=2$ and at ~ 4.7 Å for $N=18$. The Hartree distributions show a slightly lesser shift with the "cutoff" potential case being closer to the DMC ones. This is evident in Fig. 4, which displays the mean value of R, $\langle R \rangle$, as a function of the cluster size. Figure 4 also shows that the $\langle R \rangle$ computed with the "cutoff" potential approaches that obtained using DMC computations as the cluster size increases.

In summary, the Hartree energies and distributions obtained with the two modified He-He interaction potentials are close to those obtained using DMC computations. The DMC energies are better reproduced by the "truncated barrier" computations (within 3%). On the other hand, the DMC distributions are closer to the Hartree "cutoff" potential results. In what follows we present and analyze results obtained using the Hartree with the "cutoff" potential scheme.

B. Hartree results: Extension to larger cluster sizes

We performed Hartree computations for Br_2-He_N clusters over the size range $N=2$–60. In Fig. 5 we show the values of the total energies $E(N)$ and the total energies per He atom, $E(N)/N$, as a function of the cluster size N. The total energy (see also Fig. 2) and energy per atom change continuously and monotonically with the cluster size giving no indication for shell-closure effects. The energy per atom, $E(N)/N$, increases rapidly as the cluster size increases to $N \approx 15$ and then it slowly tends to the bulk value of -4.94 cm^{-1} (see, e.g., Ref. [24]), which would be, obviously, attained for

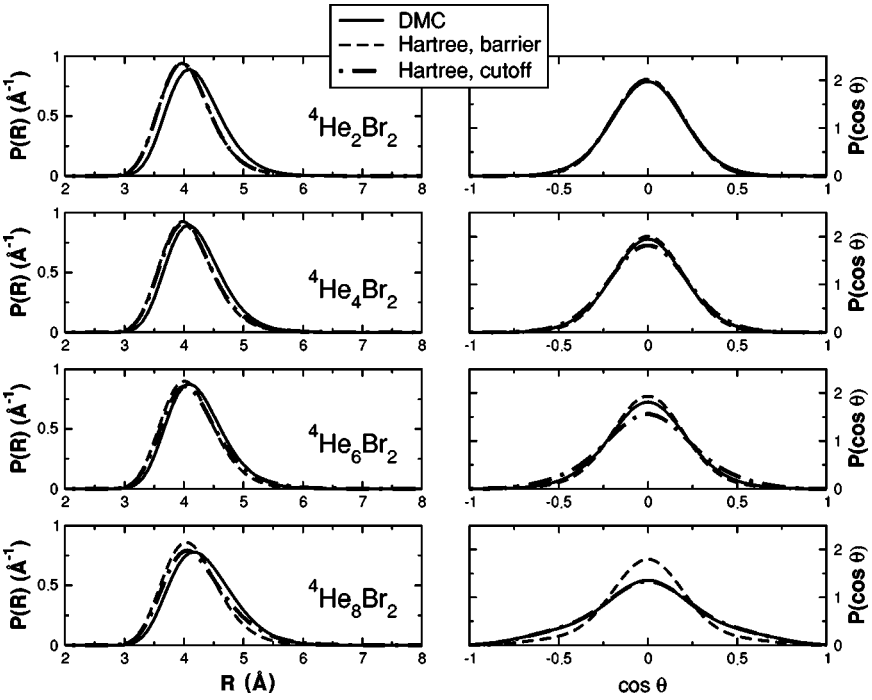

FIG. 2. Helium probability density distributions of $Br_2(X)$-$(^4He)_N$ clusters for $N=2$–8. Left panels: radial probabilities. Right panels: angular probabilities. Solid lines: DMC results. Dashed lines: Hartree with "truncated barrier" He-He potential results. Dotted lines: Hartree with "cutoff" He-He potential results. The distributions are normalized to 1.

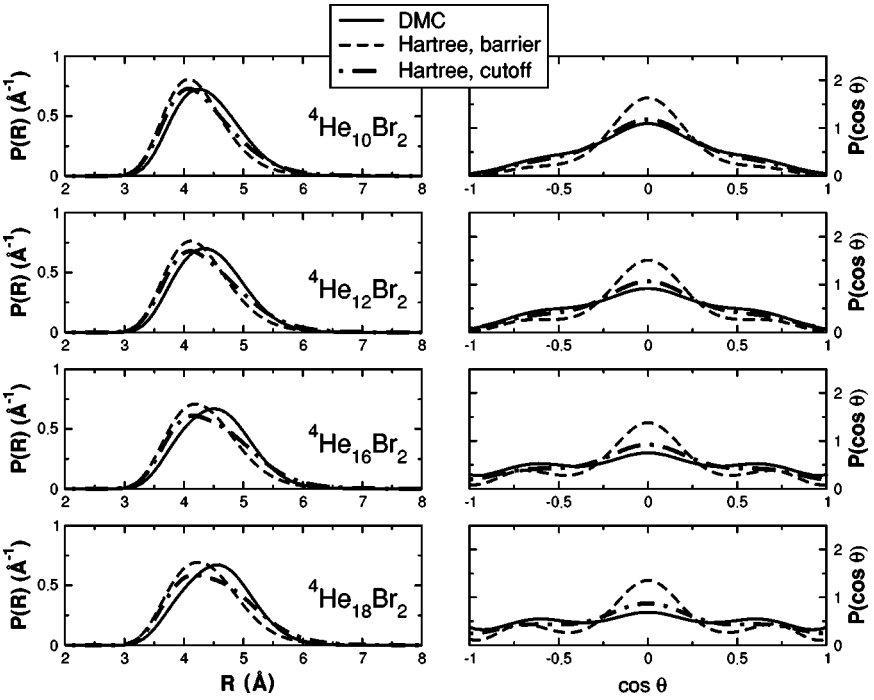

FIG. 3. Same as Fig. 2, but for cluster sizes $N=10$–18.

much larger cluster sizes than those analyzed here.

Figure 6 shows the angular density distributions for $N=2$–40 and how they become more uniform as N increases. We have also computed the occupation number distributions of the independent-particle (or, equivalently, $HeBr_2$) orbitals (given by the diagonal elements of the first-order density matrix in the independent-particle basis representation). The angular distributions for the three lowest-lying orbitals are shown in Fig. 7. The only maximum in the distribution for the lowest-energy (-18 cm^{-1}) orbital is at $\theta=90°$ (T-shaped configuration of $HeBr_2$). The distribution for the next orbital (-9 cm^{-1}) displays a minor peak around $\theta=90°$ and major peaks around $\theta\approx\pi/4$ and $3\pi/4$. The distribution for the third orbital (-7 cm^{-1}) displays peaks around $\theta=20°$, 60°, 90°, 120°. and 160°. The more removed is a peak from $\theta=90°$, the higher and broader it is.

As discussed above (cf. Fig. 2), for clusters with $N\leqslant 6$ the He atoms are located chiefly within a limited region centered at $\theta=\pi/2$. When projected on the independent-particle picture, the population of the lowest T-shaped orbital is about N in these cases. For $N=8$ the effective occupation numbers of the two lowest-energy orbitals have the values of 7 and 1, respectively, so that the two side peaks at $\theta\approx\pi/4$ and $3\pi/4$ start to get populated as well. For $N=24$, the occupation number of the third orbital is about 1, which places about 4% of the He density at peaks adjacent to $\theta=0$ and π. For $N\geqslant 30$, the He distributions are almost independent of the cluster size and they are markedly more isotropic than those for $N\leqslant 6$. The He density becomes effectively distributed over a large number of independent-boson orbitals. This can be understood by taking into account that the strongly anisotropic potential is felt mainly by the He atoms that are close

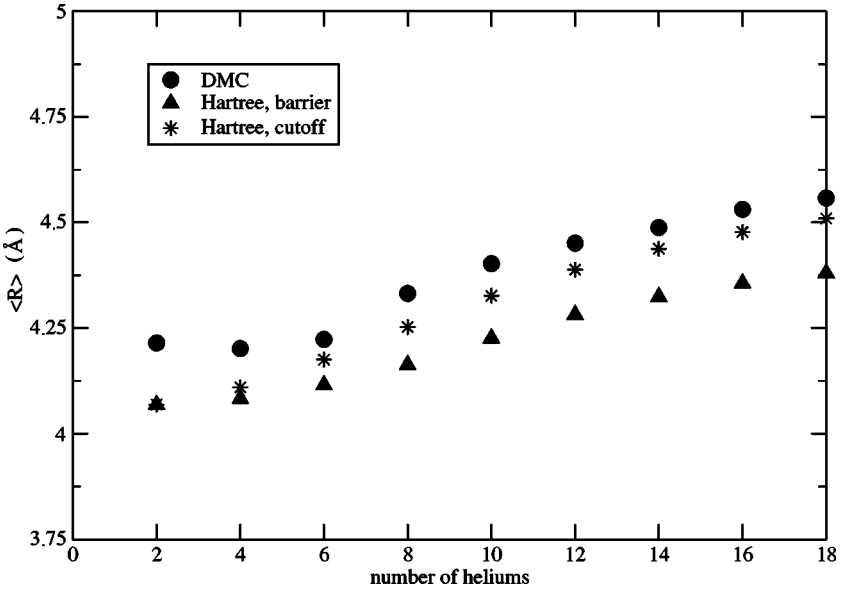

FIG. 4. Mean distances between the He and the Br_2 center of mass in $Br_2(X)$-$(^4He)_N$ clusters as a function of their size N obtained using DMC and Hartree calculations.

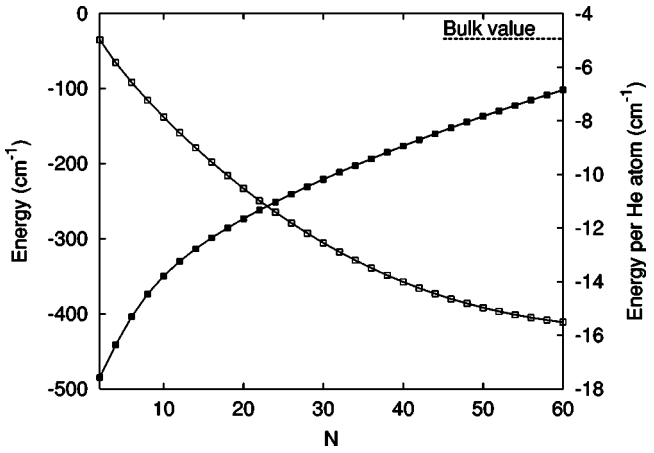

FIG. 5. Total energy $E(N)$ (open squares) and energy per He atom, $E(N)/N$ (solid squares), as a function of the cluster size N. The computations were performed using the Hartree with the "cutoff" potential scheme. The negative of the cohesive energy of the bulk ^{4}He is also shown.

to the dopant molecule whereas the spatial clustering of the He atoms more distant from the impurity is driven primarily by the He-He interaction. It thus follows that the analysis of the solvent distribution in terms of the independent-particle orbitals becomes less adequate as the size of the cluster increases.

Another aspect of the problem we have examined is the dependence of the total energy on the Br_2 bond length. We considered three bromine bond lengths $r=2.20$, 2.281, and 2.35 Å and found that for distances not too different from the equilibrium Br_2 bond length the energies can be fitted to better than 1% with a linear expression

$$E(N;r) = A(N) + B(N)r.$$

The values of the A and B parameters are plotted as a function of the cluster size in Fig. 8. Both parameters tend to a constant as the cluster size increases. The dependence of

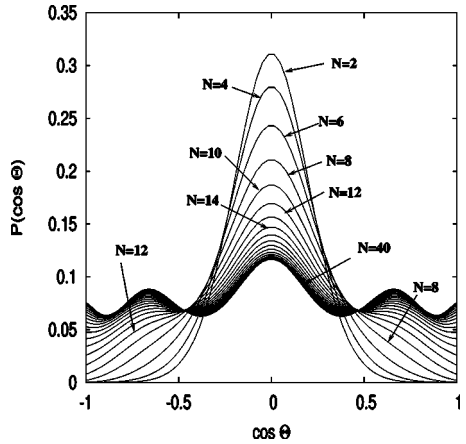

FIG. 6. Helium angular density distributions around the Br_2 molecule for different cluster sizes. The distributions are normalized to 1. The results are obtained using Hartree with "cutoff" potential computations.

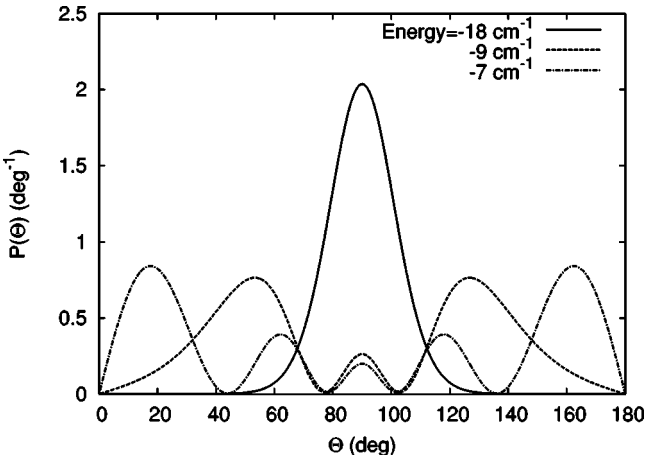

FIG. 7. Angular distributions and energies of the three lowest independent-particle picture orbitals.

the He-Br_2 interaction on the bond length distance is felt primarily by the He atoms close to the Br_2 dopant. Beyond the value $N=60$ the r dependence felt by the inner He atoms becomes insensitive to the addition of more He atoms. For larger cluster sizes, as the interaction between the He atoms that do not feel the Br_2 molecules begins to dominate the energy, the dependence of the latter on r becomes inessential.

IV. CONCLUSIONS

In this paper, we have reported results of Hartree-like model computations on the energetics and density distributions of $Br_2(X)$-$(^4He)_N$ clusters in the size range $N=2$–60. The main findings of the study can be summarized as follows.

(i) The lowest energies of the clusters are obtained for the value $\Lambda=0$ of the projection of the orbital angular momentum onto the molecular axis and the symmetric N-boson wave function—i.e., the "Σ_g" state in which all the He atoms occupy the same orbital.

(ii) The computations on small clusters ($N\leqslant 18$) show that both the energies and the probability density distributions are

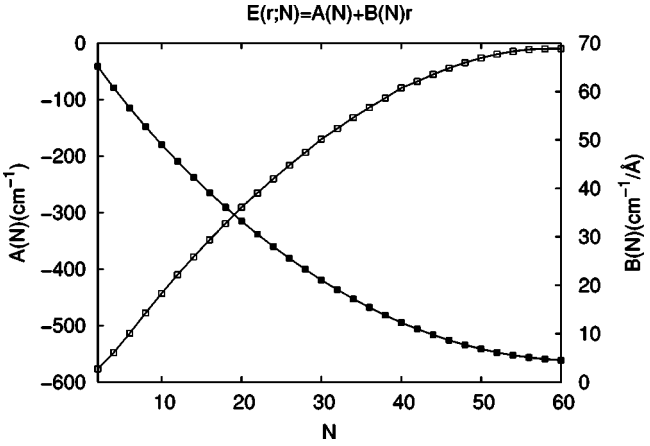

FIG. 8. Cluster size dependence for the parameters A (solid squares) and B (open squares). See the text for details.

in good agreement with those obtained in "exact" DMC computations, if the He-He short-range potential is made more realistic through use of appropriate truncation schemes.

(iii) The analysis of the angular density distributions and the occupation numbers within the independent-particle picture indicates that up to $N=6$ the solvent populates only the region of the potential minimum associated with the T-shaped configuration. For larger cluster sizes the He-He repulsion causes the He atoms to populate laterally displaced regions as well.

(iv) For $N \geqslant 30$, the angular density distribution is nearly independent of the cluster size and the Br_2 molecule is "coated" by the He solvent almost uniformly.

(v) Both the DMC and the Hartree-model ground-state energies and He density distributions change continuously and monotonically exhibiting no shell-closure effects. The energy per He atom increases monotonically to the negative of the bulk cohesive energy.

(vi) Total and single-atom energies further show a linear dependence on the Br_2 bond length. The parameters defining this dependence vary smoothly with the cluster size and asymptotically tend to constants.

It is possible that for lighter dopant molecules the dynamical correlation induced by the kinetic coupling terms, included in Eq. (1), has an effect. An intriguing question is whether this effect can lead to shell-closure phenomena. Another question is the possible role of the mixing of the Hartree products in the ground-state bosonic wave function, which was not considered here. In order to answer this question we initiated work on the full CI treatment of the ground state.

Finally, we mention that the quantum chemistry-type method used here has an advantage over density-functional-theory-based techniques because it also furnishes wave functions, which can be used to perform computations of spectra and therefore to make a better contact with the experiment. Another advantage of the approach used in this work is that unlike the DMC method it can coherently be applied for studies of fermion and mixed bosonic and fermionic doped clusters. An example is our recent work on the Raman spectra of $(He)_N$-$Br_2(X)$ clusters [13,14]. Our planned studies include extensions to polar molecules, such as CO and LiH, for which both experimental and theoretical work is available [5,25–27].

ACKNOWLEDGMENTS

This work has been partially supported by the Italy-Spain Integrated Action Programme HI02-74, DGICYT Spanish Grant No. BFM2001-2179, European TMR network Grant No. HPRN-CT-1999-0005, and Cineca (Grant No. HPRI-CT-1999-00048). F.A.G. and C.DiP. thank the Research Committee of the University of Rome *La Sapienza*. M.P.deL.-C. was supported by the "Ramón and Cajal" Programme and J.J. by the Office of Basic Energy Sciences, Division of Chemical Sciences, Geosciences, and Biosciences, U.S. Department of Energy under Contract No. W-31-109-Eng-38. M.P.deL.-C. wishes to thank C. Valdemoro, D. Alcoba, H. J. Monkhorst, and S. B. Trickey for valuable suggestions and stimulating discussions.

APPENDIX A: EVALUATION OF MATRIX ELEMENTS

We evaluate here the matrix elements of the Hamiltonian using the basis functions as defined by Eq. (19). Starting with the one-particle Hamiltonian, Eq. (2), one finds

$$\left\langle \chi^{(n\ell m)} \left| -\frac{\hbar^2}{2\mu}\frac{\partial^2}{\partial R^2} \right| \chi^{(n'\ell'm')} \right\rangle = -\frac{\hbar^2}{2\mu}\delta_{\ell\ell'}\delta_{mm'}\int_0^{+\infty} dR g_n(R;r)\frac{\partial^2}{\partial R^2} g_{n'}(R;r), \tag{A1}$$

whereas the matrix elements of the $\mathbf{l}^2$ operator are

$$\left\langle \chi^{(n\ell m)} \left| \frac{\mathbf{l}^2}{2\mu R^2} \right| \chi^{(n'\ell'm')} \right\rangle = \frac{l(l+1)}{2\mu}\delta_{\ell\ell'}\delta_{mm'}\int_0^{+\infty} dR g_n(R;r) R^{-2} g_{n'}(R;r). \tag{A2}$$

If the He-Br_2 interaction $W(r,R,\theta)$ is expanded in terms of the Legendre polynomials $P_\lambda(\cos\theta)$,

$$W(r,R,\theta) = \sum_\lambda w_\lambda(R;r) P_\lambda(\cos\theta), \tag{A3}$$

then, its matrix element is given by

$$\left\langle \chi^{(n\ell m)} | W(r,R,\theta) | \chi^{(n'\ell'm')} \right\rangle = \delta_{mm'}\left(\frac{2\ell'+1}{2\ell+1}\right)^{1/2}\sum_\lambda w_\lambda^{nn'} \langle \ell' 0, \lambda 0 | \ell\, 0\rangle \langle \ell' m', \lambda 0 | \ell\, m\rangle, \tag{A4}$$

where the terms $w_\lambda^{nn'}$ are

$$w_\lambda^{nn'} = \int_0^{+\infty} dR g_n(R;r) w_\lambda(r,R) g_{n'}(R;r) \tag{A5}$$

and $\langle \cdots, \cdots | \cdots \rangle$ denotes Clebsch-Gordan coefficients.

By denoting any He-He interaction V_{kl} appearing in Eq. (1) as $V_{12}(|\mathbf{R}_1 - \mathbf{R}_2|)$ and resorting to an expansion in terms of Legendre polynomials,

$$V_{12}(|\mathbf{R}_1 - \mathbf{R}_2|) = V_{12}(R_1, R_2\gamma) = \sum_\Lambda v_\Lambda(R_1,R_2) P_\Lambda(\cos\gamma), \tag{A6}$$

where $\cos\gamma = \mathbf{R}_1 \cdot \mathbf{R}_2 / R_1 R_2$, the two-particle matrix element can be written as

$$\langle \chi^{(n_1\ell_1 m_1)}\chi^{(n_2\ell_2 m_2)}|V_{12}|\chi^{(n_1'\ell_1' m_1')}\chi^{(n_2'\ell_2' m_2')}\rangle = \sum_{\Lambda} v_{\Lambda}^{n_1 n_2; n_1' n_2'}(-1)^{m1-m_2'}\delta_{m_1+m_2 m_1'+m_2'}\sqrt{(2\ell_1+1)(2\ell_2+1)(2\ell_1'+1)(2\ell_2'+1)}$$
$$\times \begin{pmatrix} \ell_1 & \Lambda & \ell_1' \\ 0 & 0 & 0 \end{pmatrix}\begin{pmatrix} \ell_1 & \Lambda & \ell_1' \\ -m_1 & m_1-m_1' & m_1' \end{pmatrix}\begin{pmatrix} \ell_2 & \Lambda & \ell_2' \\ 0 & 0 & 0 \end{pmatrix}\begin{pmatrix} \ell_2 & \Lambda & \ell_2' \\ -m_2 & m_2-m_2' & m_2' \end{pmatrix}, \tag{A7}$$

where $\begin{pmatrix} \cdots \\ \cdots \end{pmatrix}$ denotes $3-j$ symbols and

$$v_{\Lambda}^{n_1 n_2; n_1' n_2'} = \int_0^{+\infty}\int_0^{+\infty} dR_1 dR_2 g_{n_1}(R_1;r) g_{n_1'}(R_1;r) v_{\Lambda}(R_1,R_2) \times g_{n_2}(R_2;r) g_{n_2'}(R_2;r). \tag{A8}$$

By expressing the gradient operators in terms of spherical components

$$\nabla_0^{(i)} = \partial/\partial z_i, \quad \nabla_{\pm 1}^{(i)} = \mp(\partial/\partial x_i \pm i\,\partial/\partial y_i)/\sqrt{2},$$

where the labels $i=1,2$ are associated with the $\mathbf{R}_1$ and $\mathbf{R}_2$ vectors, the kinetic energy couplings terms in Eq. (1) take the form

$$\frac{-\hbar^2}{m_{Br_2}}\nabla_1\cdot\nabla_2 = \frac{-\hbar^2}{m_{Br_2}}\sum_{\nu=-1}^{1}(-1)^{\nu}\nabla_{\nu}^{(1)}\cdot\nabla_{-\nu}^{(2)}. \tag{A9}$$

Using the Wigner-Eckart theorem for matrix elements of $\nabla_{\pm\nu}^{(i)}$ (see, e.g., Ref. [28]),

$$\left\langle Y_{\ell\omega}\frac{f(R)}{R}|\nabla_v^{(i)}|\frac{g(R)}{R}Y_{\ell'\omega'}\right\rangle = (-1)^{-\omega}\left[\begin{pmatrix} \ell & 1 & \ell' \\ -\omega & \nu & \omega' \end{pmatrix}\Big/\begin{pmatrix} \ell & 1 & \ell' \\ 0 & 0 & 0 \end{pmatrix}\right] \times \left\langle Y_{\ell 0}\frac{f(R)}{R}|\nabla_0^{(i)}|\frac{g(R)}{R}Y_{\ell' 0}\right\rangle,$$

and taking into account that [29]

$$\left\langle \frac{f(R)}{R}Y_{\ell 0}\middle|\nabla_0\middle|\frac{g(R)}{R}Y_{\ell' 0}\right\rangle = \delta_{\ell\ell'\pm 1}[(2\ell+1)(2\ell'+1)]^{-1/2}s \times \int_0^{+\infty} dR f(R)\left[\frac{dg(R)}{dR} \mp s\frac{g(R)}{R}\right],$$

where $s=\max(\ell,\ell')$, one arrives at the following form of the matrix elements of the two-particle kinetic coupling:

$$\frac{-\hbar^2}{m_{Br_2}}\left\langle \chi^{(n_1\ell_1 m_1)}\chi^{(n_2\ell_2 m_2)}|\boldsymbol{\nabla}_1\cdot\boldsymbol{\nabla}_2|\chi^{(n_1'\ell_1' m_1')}\chi^{(n_2'\ell_2' m_2')}\right\rangle = \frac{-\hbar^2}{m_{Br_2}}\sum_{\nu=-1}^{1}(-1)^{-\nu}\prod_{i=1}^{2}(-1)^{-m_i}\left[\begin{pmatrix} \ell_i & 1 & \ell_i' \\ -m_i & \nu & m_i' \end{pmatrix}\Big/\begin{pmatrix} \ell_i & 1 & \ell_i' \\ 0 & 0 & 0 \end{pmatrix}\right]\delta_{\ell_i\ell_i'\pm 1}$$
$$\times[(2\ell_i+1)(2\ell_i'+1)]^{-1/2}s_i\int_0^{+\infty} dR_i g_{n_i}(R_i;r)\left[\frac{dg_{n_i'}(R_i;r)}{dR_i} \mp s_i\frac{g_{n_i'}(R_i;r)}{R_i}\right]. \tag{A10}$$

APPENDIX B: EVALUATION OF DISTRIBUTIONS

The helium radial density distributions are given by

$$D(R) = \sum_{(n\ell m)}\sum_{(n'\ell' m')}\delta_{\ell\ell'}\delta_{mm'}g_n(R;r)g_{n'}(R;r)P_{n\ell m,n'\ell' m'}, \tag{B1}$$

where $P_{n\ell m,n'\ell' m'}$ are the elements of the first-order reduced density matrix. In order to evaluate the helium angular helium density distributions we assume an expansion in Legendre polynomials,

$$D(\cos\alpha) = \sum_n d_n P_n(\cos\alpha), \tag{B2}$$

where

$$d_n = \frac{2n+1}{2}\langle\Phi_{\Lambda}^{(N)}|P_n(\cos\alpha)|\Phi_{\Lambda}^{(N)}\rangle \tag{B3}$$

and

$$\langle\Phi_{\Lambda}^{(N)}|P_n(\cos\alpha)|\Phi_{\Lambda}^{(N)}\rangle = \sum_{(n\ell m)}\sum_{(n'\ell' m')}\delta_{nn'}\delta_{mm'}\left(\frac{2\ell'+1}{2\ell+1}\right)^{1/2} \times\langle\ell' 0, n0|\,\ell\,0\rangle\langle\ell' m', n0|\,\ell\, m\rangle P_{n\ell m,n'\ell' m'}. \tag{B4}$$

It is convenient to compute the total angular momentum distribution $P(L_N)$ by starting with the uncoupled representation which gives the weights of the states $\langle \ell_1 m_1 \cdots \ell_i m_i \cdots \ell_N m_N \rangle$. For the special case of N bosons occupying the same orbital $m=0$,

$$P(\ell_1 \cdots \ell_i \cdots \ell_N) = P(\ell_1) \cdots P(\ell_i) \cdots P(\ell_N), \tag{B5}$$

where

$$P(\ell_i) = \sum_{(n\ell m)} \delta_{\ell \ell_i} P_{n\ell m, n\ell m}. \tag{B6}$$

Then the weight of the two-body angular momentum L_2 in the $\Phi_0^{(N)}$ wave function can be computed as

$$P(L_2) = \sum_{\ell_2} \sum_{\ell_1} \langle \ell_2 0, \ell_1 0 | L_2 0 \rangle^2 P(\ell_2) P(\ell_1), \tag{B7}$$

for the three-body angular momentum L_3 as

$$P(L_3) = \sum_{\ell_3} \sum_{L_2} \langle \ell_3 0, L_2 0 | L_3 0 \rangle^2 P(\ell_3) P(L_2), \tag{B8}$$

and for the total, N-body, angular momentum L_N as

$$P(L_N) = \sum_{l_N} \sum_{L_{N-1}} \langle \ell_N 0, L_{N-1} 0 | L_N 0 \rangle^2 P(\ell_N) P(L_{N-1}). \tag{B9}$$

[1] For a recent review see, J. P. Toennies, and A. F. Vilesov, Angew. Chem., Int. Ed. **43**, 2622 (2004).
[2] S. Grebenev, J. P. Toennies, and A. F. Vilesov, Science **279**, 2083 (1998).
[3] J. Tang, Y. Xu, A. R. W. McKellar, and W. Jäger, Science **297**, 2030 (2002).
[4] J. Y. Xu and W. Jäger, J. Chem. Phys. **119**, 5457 (2003).
[5] J. Tang and A. R. W. McKellar, J. Chem. Phys. **119**, 754 (2003).
[6] J. Tang and A. R. W. McKellar, J. Chem. Phys. **119**, 5467 (2003).
[7] C. Callegari, K. K. Lehmann, R. Schmied, and G. Scoles, J. Chem. Phys. **115**, 10 090 (2001).
[8] *Quantum Monte Carlo Methods in Physics and Chemistry*, Vol. 525 of NATO Series, Mathematical and Physical Sciences, edited by P. Nightingale and C. J. Umrigar, (Kluwer Academic, Boston, 1999).
[9] *Simulation of Liquids and Solids. Molecular Dynamics and Monte Carlo Methods in Statistical Mechanics*, edited by G. Ciccotti, D. Frenkel, and I. R. McDonald, (North-Holland, Amsterdam, 1987).
[10] P. Jungwirth and A. I. Krylov, J. Chem. Phys. **115**, 10 214 (2001).
[11] A. Heidenreich and J. Jortner, J. Chem. Phys. **115**, 10 175 (2001).
[12] M. Barranco, M. Pi, S. M. Gatica, E. S. Hernández, and J. Navarro, Phys. Rev. B **56**, 8997 (1997).
[13] D. López-Durán, M. P. de Lara-Castells, G. Delgado-Barrio, P. Villarreal, C. Di Paola, F. A. Gianturco, and J. Jellinek, J. Chem. Phys. **121**, 2975 (2004).
[14] D. López-Durán, M. P. de Lara-Castells, G. Delgado-Barrio, P. Villarreal, C. Di Paola, F. A. Gianturco, and J. Jellinek, Phys. Rev. Lett. **93**, 053401 (2004).
[15] C. Di Paola, F. A. Gianturco, D. López-Durán, M. P. de Lara-Castells, G. Delgado-Barrio, P. Villarreal, and J. Jellinek (unpublished).
[16] R. N. Zare, A. L. Schmeltekopf, W. J. Harrop, and D. L. Albritton, J. Mol. Spectrosc. **46**, 37 (1973).
[17] J. Fernández-Rico, in *Self-Consistent Field, Theory and Applications*, edited by R. Carbó and M. Klobukowski, Vol. 70 of *Physical and Theoretical Chemistry* (Elsevier, New York, 1990).
[18] J. Fernández-Rico, J. M. García de la Vega, M. Paniagua, and J. I. Fernández-Alonso, J. Chem. Phys. **79**, 4407 (1983).
[19] K. P. Huber and G. Herzberg, *Constants of Diatomic Molecules* (Van Nostrand Reinhold, New York, 1979).
[20] T. González-Lezana, M. I. Hernández, G. Delgado-Barrio, A. A. Buchachenko, and P. Villarreal, J. Chem. Phys. **105**, 7454 (1996).
[21] R. Prosmiti, C. Cunha, P. Villarreal, and G. Delgado-Barrio, J. Chem. Phys. **116**, 9249 (2002).
[22] Z. Bačić, M. Kennedy-Mandzink, J. W. Moskowitz, and K. E. Schmidt, J. Chem. Phys. **97**, 6472 (1992).
[23] N. Bernardes and H. Primakoff, Phys. Rev. **119**, 968 (1960).
[24] M. H. Kalos, M. A. Lee, P. A. Whitlock, and G. V. Chester, Phys. Rev. B **24**, 115 (1981).
[25] F. Paesani and F. A. Gianturco, J. Chem. Phys. **116**, 10 170 (2002).
[26] P. Cazzato, S. Paolini, S. Moroni, and S. Baroni, J. Chem. Phys. **120**, 9071 (2004).
[27] K. Nauta and R. E. Miller, J. Chem. Phys. **113**, 10 158 (2000).
[28] A. R. Edmonds, *Angular Momentum in Quantum Mechanics* (Princeton University Press, Princeton, 1957).
[29] P. Villarreal, O. Roncero, and G. Delgado-Barrrio, J. Chem. Phys. **101**, 2217 (1994).